

**DEVELOPMENT OF A TIME OF FLIGHT
MASS SPECTROMETRY METHOD FOR THE
SCREENING OF POLYCYCLIC AROMATIC
HYDROCARBONS AND NITRO-
SUBSTITUTED POLYCYCLIC AROMATIC
HYDROCARBONS**

**FINAL REPORT
CONTRACT NO. 97-305**

PREPARED FOR:

**CALIFORNIA AIR RESOURCES BOARD
RESEARCH DIVISION
1001 I STREET
SACRAMENTO, CA 95814**

PREPARED BY:

**J. SURO
Q. CHEN
P. B. KELLY**

**DEPARTMENT OF CHEMISTRY
UNIVERSITY OF CALIFORNIA, DAVIS
DAVIS, CA 96161**

APRIL 2000

For more information about the ARB's, Research Division's
research and activities, please visit our Website:

<http://www.arb.ca.gov/research/research.htm>

Disclaimer

The statements and conclusions in this report are those of the University of California at Davis and not necessarily those of the California Air Resources Board. The mention of commercial products, their source, or their use in connection with material reported herein is not to be construed as actual or implied endorsement of such products.

Abstract

Laser Desorption Ionization Time of Flight Mass Spectrometry LDI/TOFMS has been developed for the direct screening of polycyclic aromatic hydrocarbons (PAHs) and nitro-substituted polycyclic aromatic hydrocarbons (nitro-PAHs). An ultraviolet 266-nm laser desorbs and ionizes PAHs and nitro-PAHs from the filter support material. The ions are mass analyzed in a custom built time of flight mass spectrometer. The laser power dependence of ionization and fragmentation of positive ions for the PAH compounds listed in ARB method 429 has been examined. The negative ion yield of nitro-PAH that was targeted by the MLD source test method has also been systematically examined for fragmentation and ionization efficiency.

The fragmentation / ionization studies show that there is a range of power densities that can produce molecular ion without significant fragmentation of the parent molecule for all but three of the compounds listed in Method 429. Naphthalene, acenaphthalene and acenaphthene have relatively high vapor pressures. The vapor pressure makes analysis of the three small PAH compounds very difficult by LDI/TOFMS, however these are the three compounds most easily detected by GC/MS. The optimal 266 nm laser power densities for detection and identification of different PAHs and nitro-PAHs are similar.

Using laser power densities ranging from 1.3 to 2.4×10^6 W/cm² it is possible to screen ambient samples for detection of a wide range of PAHs and nitro-PAHs. The listed nitro-PAHs yield [M – NO]⁺ as the most identifiable marker; in the case of 5-nitroacenaphthene and 2-nitrofluorene, [M – H]⁺ product ion serves as identifier.

Table of Contents

| | | |
|------|---|----|
| I. | Introduction | 5 |
| II. | Laser Desorption Ionization Time of Flight Mass Spectrometry | 7 |
| | II.1 Laser Induced Desorption Photo-ionization | 7 |
| | II.2 Time of Flight Mass Spectrometry | 8 |
| III. | Experimental | 10 |
| | III.1 Experimental Apparatus | 10 |
| | III.2 Sample Preparation of Standard Compounds | 11 |
| | III.3 Systematic Variation of Laser Power Density. | 13 |
| IV. | Results | 14 |
| | IV.1 Optimal Power Density | 14 |
| | IV.2 Spectra of PAHs | 16 |
| | IV.3 Spectra of Nitro-PAHs | 20 |
| | IV.4 Matrix effects | 26 |
| V. | Conclusions | 28 |
| VI. | References | 31 |
| | Appendix A. Time of flight | 32 |
| | Appendix B. Mass calibration of ion spectra | 34 |
| | Appendix C. Selected information | 36 |
| | Table C.1 Molecular formulas and structures of PAHs | 36 |
| | Table C.2 Molecular formulas and structures of nitro-PAHs | 38 |
| | Table C.3 Electron affinity of selected atoms and molecules | 39 |
| | Appendix D. Characterization of chemical composition and size of diesel exhaust particulate matter by LDITOF/MS | 40 |

I. Introduction

Polycyclic Aromatic Hydrocarbons and nitro-substituted Polycyclic Aromatic Hydrocarbons (PAHs and nitro-PAHs) are found in particles that originate from the incomplete combustion of hydrocarbons. Diesel engines and electric power plants are two examples of sources of such particulate matter. Several of the PAHs and nitro-PAHs considered in this work have been identified as carcinogenic and potentially carcinogenic compounds [1,2]. The presence of the aromatic compounds in the air is a potential hazard to human health.

Traditional methods for the determination of PAHs and nitrated PAHs have been based on gas chromatography/mass spectrometry or liquid chromatography with fluorescence techniques for detection; both approaches are time consuming, expensive, and difficult to implement for the continuous monitoring of PAHs and nitro-PAHs. There is a need for a method for rapid detection and identification of PAHs and derivative compounds on air sampling filters. We have developed a Laser Desorption Ionization Time of Flight Mass Spectrometry (LDI/TOFMS) technique that provides a means of rapid screening of particulate matter samples for those classes of compounds with no extraction or separation steps. The method employs pulsed laser light of 266 nm that desorbs and ionizes PAHs and nitro-PAHs compounds on particulate matter filters, the ions that are formed are extracted from the source using electric fields, and directed to a multi channel plate detector. The time of flight that takes for an ion to reach the detector is proportional to its mass (see section II.2).

The work performed on PAHs and nitro-PAHs (see section IV) includes the characterization of their response to ultra violet radiation (UV) of 266 nm. The overall optimal

laser power density that is suitable for the detection and identification of those compounds in particulate matter filters have been determined. Using a consistent range of power densities (1.3 to 2.4×10^6 W/cm²) it is possible to detect and identify all PAHs and nitro-PAHs (with the exception of three PAHs, naphthalene, acenaphthalene and acenaphthene, whose high vapor pressure make them unsuitable for this kind of analysis). Our work demonstrates that it is possible to consider an implementation of the LDI/TOFMS technique as a method for the direct screening of PAHs and nitro-PAHs on particulate matter filters based on a commercial TOF instrument.

The LDI/TOFMS technique outlined above has the advantage of minimal sample preparation; without extraction and separation steps that are necessary in GC/MS. Consequently, the actual analysis takes a short time (less than 5 minutes per sample), thus reducing cost. LDI/TOFMS could be used to rapidly identify samples which contain detectable levels of a PAH or nitro-PAH compound, from those without significant content, reserving a full EPA quantitative analysis for those samples containing PAHs and nitro-PAHs.

In this report the experimental details of the technique and the work performed are described. In section IV Results, the spectra of selected PAHs and nitro-PAHs are examined in detail. LDI/TOFMS is demonstrated to be a technique that is applicable for screening of environmental samples for PAHs compounds and is the subject of continuing study.

Recent success with the TOF mass spectroscopic analysis of diesel particulate matter sized using an impactor is included in Appendix D. The success of the analysis of particulate matter in the five size ranges from 2.5 micron to ultra fine demonstrates the capability of application of TOF mass spectroscopy to applied problems in combustion analysis.

II. Laser Desorption Ionization Time of Flight Mass Spectrometry

II.1 Laser Induced Desorption Photo-ionization

In laser desorption ionization time of flight mass spectrometry (LDI/TOFMS), a laser pulse is used to desorb and ionize material from the target surface (see Figure 1). The process is characterized by rapid heating of the surface to vaporize the condensed phase material, giving

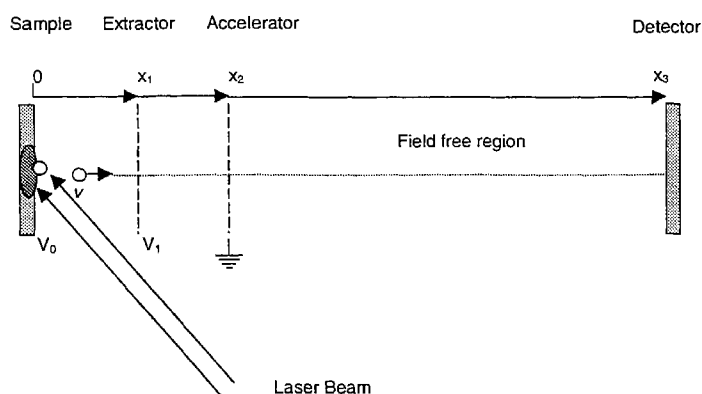


Figure 1. Schematic diagram of the LDITOF/MS. A 266 nm laser shot hits a sample at 45 degrees. The ions thus formed are repelled by the source plate at potential V_1 and directed towards the detector. A extraction plate at a potential V_2 ($V_2 < V_1$), is used for establishing a uniform electric field at the source region and enhance the mass resolution.

rise to formation of a plume of desorbed material containing ions, electrons, and neutral molecules. Ionization of molecules of interest is enhanced by the use of laser light with photon energies that correspond to molecular excited electronic states. The ions thus formed are extracted using a continuous electric field that directs the ions towards a detector through a field free region. When UV laser light of 266 nm is used for LDI process, the ion formation mechanism is dominated by resonant two-photon ionization of PAHs and PAHs derivatives [3]. Two 266 nm photons put 9.32 eV of energy in the absorbing molecule. For most of PAHs and derivatives, the ionization energy is in the range of 7 to 9 eV. Formation of positive ions resulting from resonant or multiphoton absorption can be described by (eq. 1):



PAHs form stable positive parent ions due to the stability of the aromatic electronic structure.

rise to formation of a plume of desorbed material containing ions, electrons, and neutral molecules. Ionization of molecules of interest is enhanced by the use of laser light with photon energies that correspond to molecular excited electronic states. The ions thus formed are extracted using a continuous electric field that directs the ions towards a detector through a

Free electrons (eq. 1) created in the process of photo-ionization will collide with molecules in the plume. The frequency of electron-molecule collisions depends on the density of molecules in the desorbed plume and density of electrons. Multiple collisions lead to a population of thermalized electrons that can be captured either via resonant electron capture (eq. 2) or dissociative electron capture (eq. 3):



Electron-molecule collisions and anion-molecule collisions are sufficiently high in the dense regions of the plume such that anion formation is controlled by thermodynamic factors. The electron affinities of the neutral molecules determine the probability of anion formation. The neutrals are desorbed in substantial excess relative to the number of electrons. The desorbed molecules compete to capture electrons and compounds with high electron affinities, such as nitro-PAHs, are likely to capture the free electrons to yield stable anions.

Efficient detection of molecular ions needed for analytical work requires a careful balancing of laser power effects. Increasing laser power yields increased desorption of molecules from the surface, but also yields increased fragmentation that obscures the analysis. However as it is detailed in section III of this report, using power densities with levels in the range of 1.3 to 2.4×10^6 W/cm², the fragmentation phenomena is minimized for the compounds of interest.

II.2 Time of Flight Mass Spectrometry

In conventional LDI/TOFMS, static electric fields are used (see Figure 1) for the extraction of the ions formed by the action of the laser light at the source. The ions are formed in a well-defined region irradiated by the laser light. An electrostatic field in the source area accelerates the ions down the flight tube to the detector. The total energy gained by an ion depends on its charge. For an ion of charge q and mass m , the total gain of kinetic energy in the source region is:

$$\Delta E_x = q|\Delta V| = \frac{1}{2}mv^2 \quad \text{eq. 4}$$

Where v is the velocity of the ion at the exit of the source region. ΔV is the total electric potential drop across the source.

In the field free region, an ion moves with constant speed. Typically the source region is very small when compared to the field free region, then the total time of flight of an ion from the source to the detector is approximately the time of flight in the field free region. This time $\Delta t = x_3/v$ (see Figure 1) is:

$$\Delta t \equiv \frac{x_3}{(2V)^{1/2}} \left(\frac{m}{q} \right)^{1/2} \quad \text{eq.5}$$

From where the ratio m/q is proportional to Δt^2 . Ions with different mass/charge ratio (charge usually is 1 electronic charge) arrive at the detector at different times (See Appendix A for more details).

III. Experimental

III.1 Apparatus

Laser desorption ionization mass spectra were obtained by using a custom-built time of

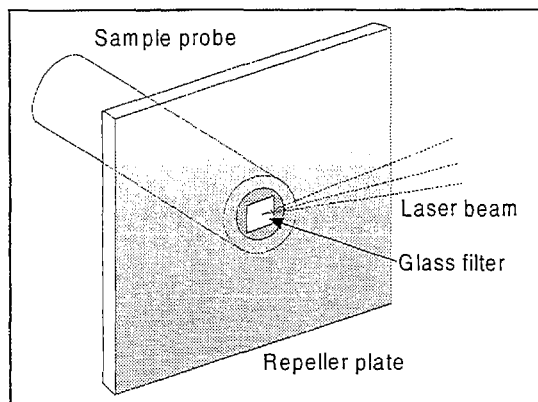


Figure 2. A 266 nm laser beam pulse making an angle of 45° hits the sample deposited onto glass fiber. The ions thus formed are repelled from the source by the electric field.

flight mass spectrometer operating in the linear mode. The source ion optics (R.M. Jordan, Grass Valley, CA), are equipped with acceleration, extractor, and repeller plates based upon the Wiley-McLaren [4] design (see Figure 1). Samples were inserted through a fast pump-down load-lock into the source region. The sample probe consists of an aluminum cylinder whose tip has been shaped to fit into the repeller plate, see Figure 2. The tip of the probe (area 25 mm^2) can be rotated to allow analysis at multiple positions on the sample probe.

Typically operating pressure was 2×10^{-6} Torr, which is achieved with diffusion pumps, equipped with cryotraps.

Pulsed ultraviolet radiation at 266 nm was used to desorb and ionize the sample. The 266 nm radiation is the fourth harmonic of a Spectra Physics (Mountain View, CA) Quanta Ray DCR-3 Nd:YAG laser with an 8 ns pulse width. The UV laser beam was focused into the source region through a 250 nm focal length S1-UV quartz lens. The beam was incident to the sample surface at 45° . Laser energy was measured by using a Molectron (Portland, OR) model J9LP joulemeter interfaced to a PcJ meter (Q & A Instruments, Glendale, AZ). Laser energy typically ranged from 0.5 to 7.5 $\mu\text{J}/\text{pulse}$ operating at 5 Hz, yielding maximum power densities on the order of 10^6 to $10^7 \text{ W}/\text{cm}^2$ on 90-micron diameter spot at the focus. Typical resolution ($M/\Delta M$) for these experiments was 100 (full width at half maximum, FWHM).

The time of flight mass spectrometer section of the apparatus (see Figure 1) consists of a source/repeller plate, extractor and accelerator grids. For extraction and analysis of positive ions (PAHs), the following electric potential were applied: repeller = 4.5 kV; extractor = 1.5 kV; accelerator and drift tube = 0.0 kV. For negative ion extraction and analysis, potentials of -4.5 and -1.5 kV were applied to repeller and extractor respectively.

Either positive or negative ions extracted using the proper bias, were detected at the end of the field free drift tube using a dual microchannel plate (MCP) detector held at -2.0 kV (+2.0 kV for negative ions). The current generated at the MCP detector was 50 Ω terminated into a 100 MHz transient recorder (DSP model 2001 AS transient recorder) and digitized with 8-bit precision. Spectra were recorded in 4k channels with a 10 ns bin resolution, corresponding to 40 μ s acquisition time per spectrum. Signals from 50-100 laser pulses were averaged by a DSP (Fremont, CA) model 4101 averaging memory and transferred via computer-automated measurement and control (CAMAC) interface to a microcomputer. Data acquisition and subsequent analysis were performed by using a standard personal computer controlled by software developed in-house [5,6].

III.2 Sample Preparation of Standard Compounds

PAHs and nitro-PAHs standards compounds (98%-99% purity) were obtained from several companies (Aldrich, AccuStandard, ChemSyn Lab.) and used without further purification. Stock solutions were prepared at concentrations of 0.1-0.2 mg/mL in methanol. Aliquots (15 μ L) of standard solution were deposited onto glass fiber air-sampling filter (Gelman Type A/E), fixed to the sample probe with double-sided adhesive tape. LDI mass spectra of blank filters displayed no background mass spectra over the range of laser powers used. The Gelman type A/E filters are commonly used for PM 2.5 and PM 10 air sampling.

On the tip circular flat area of 25 mm² of the probe, a double-sided adhesive tape was used for placing square 2 mm X 2 mm pieces of glass filter. The compounds in solution were deposited by using clean disposable pipettes to prevent contamination.

The procedure described above was followed for the preparation of all the samples. Assuming a uniform distribution on the surface of the filter, a sample would have a compound density of 1 g/m^2 . When considering the area of the laser spot on the sample, the total amount of material exposed is about 6 ng (or a few tens of picomole of PAHs). Detection of compounds in samples prepared as above, defines a detection limit of at least 6 ng using LDI/TOFMS.

III.3 Systematic Variation of Laser Power Density.

The response of PAHs and nitro-PAHs to different laser powers was systematically examined. In order to find the optimal energy densities necessary for detection and identification

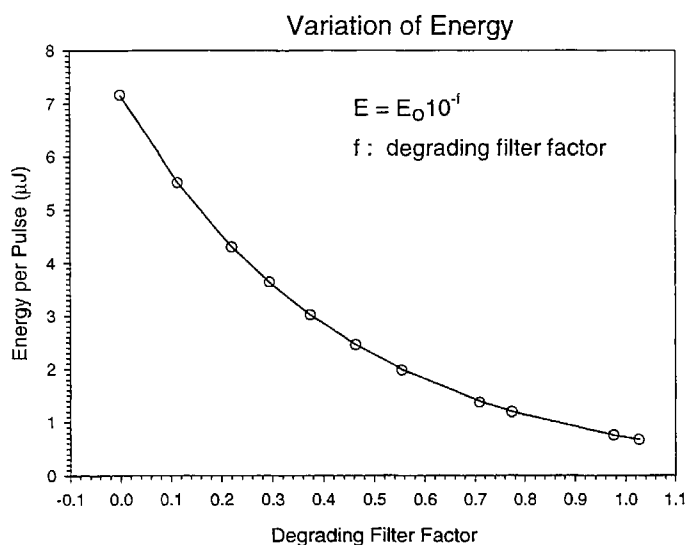


Figure 3. Variation of the energy per pulse applied to the sample. Using a set of 10 neutral density optical filters, the initial intensity of the laser is reduced. The intensity decays according to a exponential decay base 10. The value of the filter is the exponent of the function.

of parent ions, samples of each compound were subject to 11 different laser power densities.

The laser was set up to deliver 7.17 μJ per pulse to the system. Laser power incident on the sample was varied from 0.67 to 7.17 μJ by insertion of neutral density optical filters. In Figure 3, the height of each circle represents the energy per pulse applied to the sample when a corresponding neutral density filter was used. The energy decays with the attenuation factor according to equation 6:

$$E = E_0 10^{-f} \quad \text{eq.6}$$

Where E_0 is the initial energy per pulse of the laser beam, and f is the attenuation factor of the filter. Laser energy fluctuates from pulse to pulse, however in average (over 50 shots) the energy remains constant during data taken of a spectrum. During long experimental sessions, average energy shifting was detected up to a maximum of 10 %. Filters used in this work ranged from $f=0.1$ to $f=1.0$. The attenuation factor of each filter was measured and corrected from their nominal values.

The use of neutral density filters achieved systematic variation of laser power without variation of pulse shape or timing characteristics.

IV. Results

IV.1 Optimal Power Density

A screening technique for PAHs and nitro-PAHs based on LDI/TOFMS needs to be sensitive and direct, without sample preparation. The main objective of our work has been to find

Table I. Power Densities Used.

| Neutral Density Filter | Power Density (W/cm ²) |
|------------------------|------------------------------------|
| 0.00 | 14.1X10 ⁶ |
| 0.11 | 10.8X10 ⁶ |
| 0.22 | 8.49X10 ⁶ |
| 0.30 | 7.14X10 ⁶ |
| 0.38 | 5.94X10 ⁶ |
| 0.46 | 4.84X10 ⁶ |
| 0.56 | 3.92X10 ⁶ |
| 0.71 | 2.75X10 ⁶ |
| 0.77 | 2.37X10 ⁶ |
| 0.98 | 1.49X10 ⁶ |
| 1.03 | 1.32X10 ⁶ |

the optimal range of power densities necessary for molecular ion detection of PAHs and nitro-PAHs. We also characterize the range of power densities for which fragmentation of the parent ion becomes important. Our results indicate that samples containing different chemicals can be examined using an optimal laser power.

In order to determine the optimal range of laser intensity, the ion yield was examined under 11 power densities. The area irradiated by the laser in each sample was always the

same: a circle of 90-micron diameter. Using neutral density optical filters, the intensity of the laser was varied (see section III.3), producing power densities ranging from 1.3×10^6 to 14.1×10^6 W/cm² on the sample, see Table I. Typically spectra were taken averaging the ion yield of 50 laser shots.

Positive ion spectra of Chrysene obtained using 9 energy power densities are displayed in Figure 4. Chrysene shows a strong parent ion signal, however fragmentation into carbon chains becomes very important at the higher power densities used in the sequence of increasing laser power. As the power density goes down, a clear and very well resolved parent ion peak appears, allowing an easy identification and detection. When intense laser powers are used, high ion yield produces undesired effects such as intense space charge effect at the source region that causes a

Chrysene

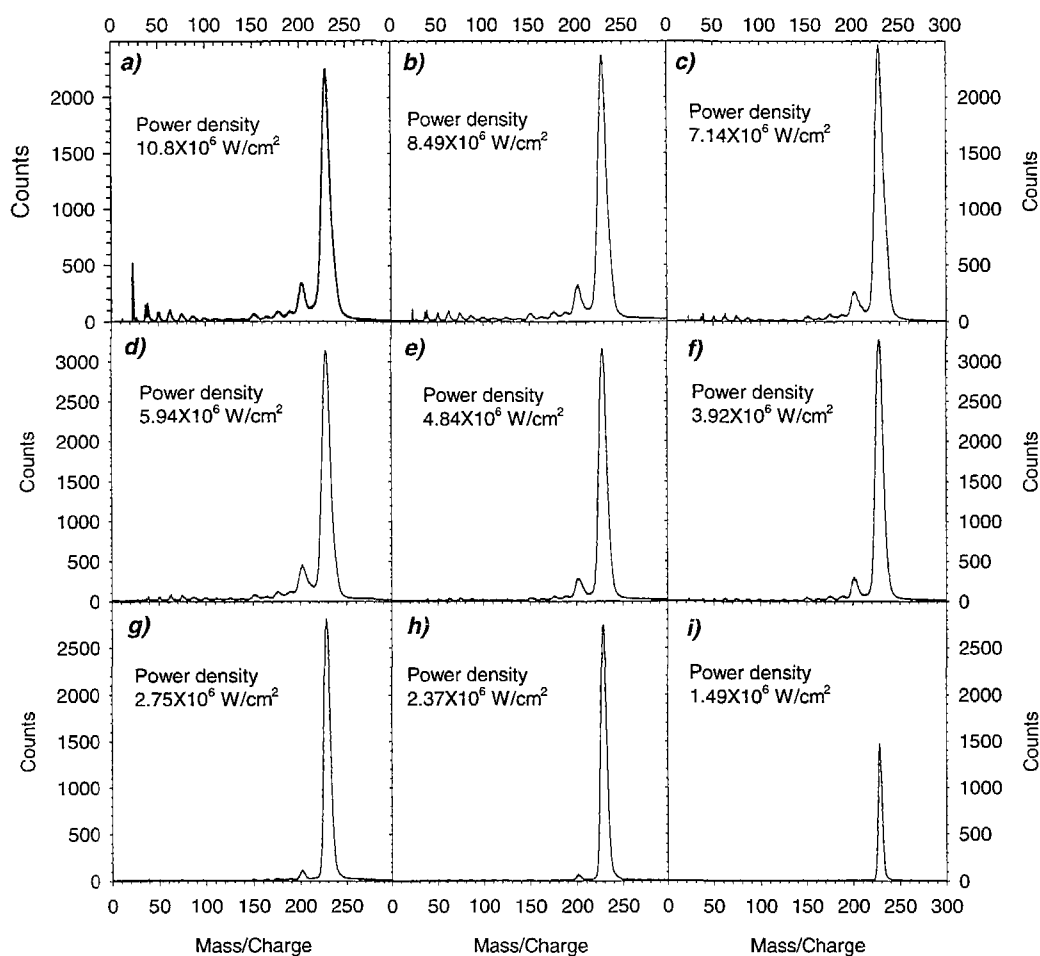


Figure 4. Positive ion yield of chrysene. From plot a) to i), lower laser power densities produce less fragmentation of the parent ion (mass 228.29 a.m.u.). Laser power densities of $1.5 \times 10^6 \text{ W/cm}^2$ generate parent ions without significant fragmentation; however total ion yield is reduced.

large shift in the calibration constants. Another effect of excessive laser power is a broadening of the ion peaks due to multiple collisions in a dense plume of desorbed material and ions. In the case of Chrysene, the strong parent ion was observed even at relatively high laser powers, Figure 4a). For most of the PAHs examined, use of high laser powers, produces abundant low mass

fragments and a broadening of the parent ion accompanied by a reduction of the parent ion intensity.

The response observed in *g*), *h*) and *i*) of Figure 4 for Chrysene is typical of all PAHs investigated in this work. Power densities in the range of $1.3 \sim 1.5 \times 10^6$ W/cm² yield parent ions with virtually no fragmentation.

The PAHs of interest share similar ionization and fragmentation characteristics. All PAHs of Table II are readily photo ionized by 266 nm radiation yielding parent positive ions.

IV.2 Spectra of PAHs

The compounds of interest fall into two groups of compounds, polycyclic aromatic compounds (PAHs) and nitro-derivatives of PAHs. The complete list of PAHs investigated in this work appears in Table II (see structure and molecular formula at Appendix C). These compounds are listed in the Target Analytes of ARB Method 429.

Table II

Method 429 Target Analytes

| | |
|---------------------|------------------------|
| Naphthalene | Chrysene |
| 2-Methylnaphthalene | Perylene |
| Acenaphthene | Benzo[b]fluoranthene |
| Acenaphthalene | Benzo[k]fluoranthene |
| Fluorene | Benzo[a]pyrene |
| Phenanthrene | Benzo[e]pyrene |
| Anthracene | Benzo[ghi]perylene |
| Fluoranthene | Indeno[1,2,3-cd]pyrene |
| Pyrene | Dibenz[a,h]anthracene |
| Benzo[a]anthracene | |

All the compounds in Table II produced abundant molecular ions with 266-nm radiation at low power levels. Figure 5 illustrates the production of positive molecular ions for pure samples of several PAHs with laser power densities range from 1.3 and 2.7×10^6 W/cm². Mass resolution ($M/\Delta M$) varies with each compound but each PAH yields a significant parent ion.

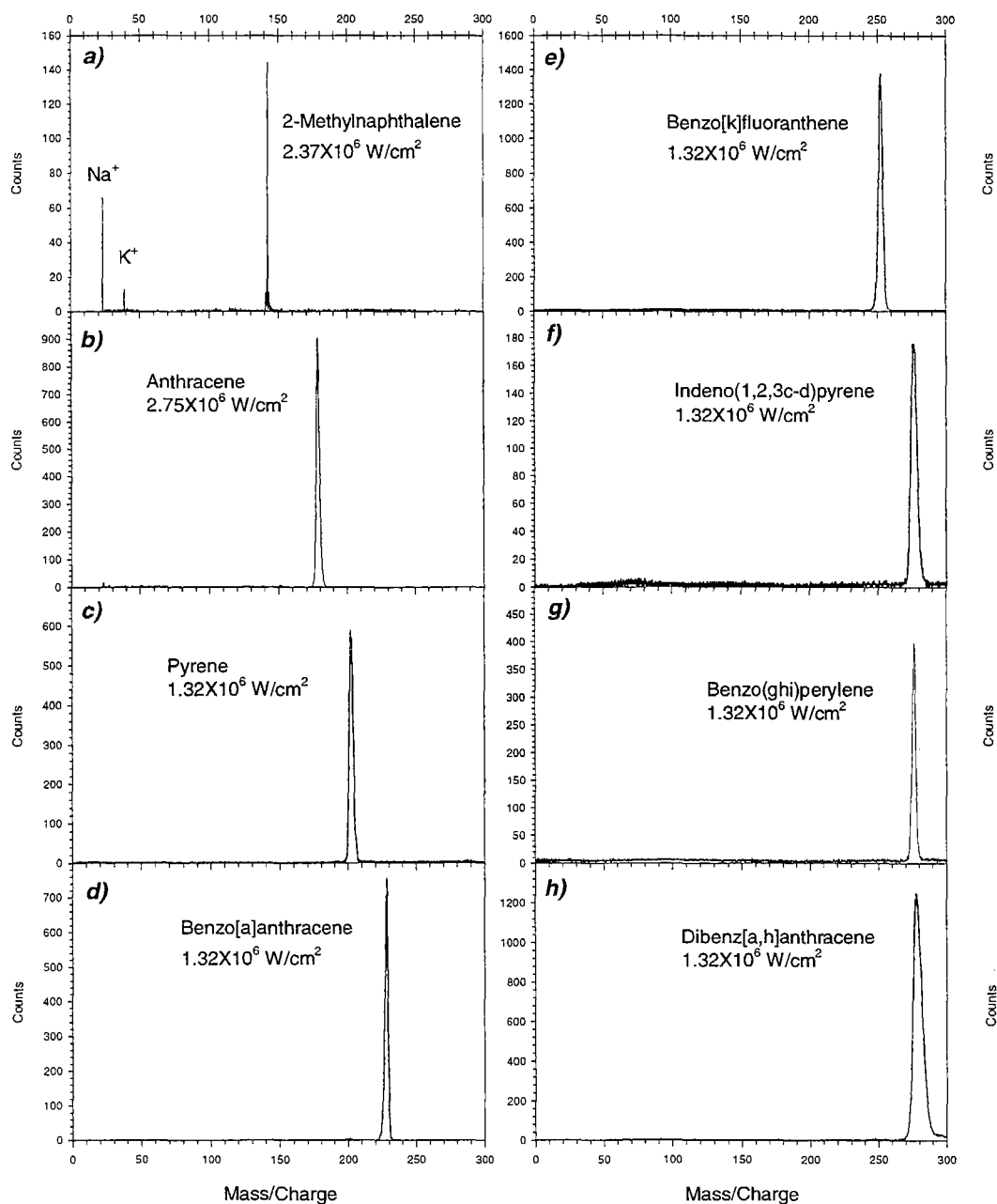


Figure 5. Positive ion yield spectra of 8 PAHs listed in Table II. When the power density is low enough, there is virtually no fragmentation. Resolution ($M/\Delta M$) varies from compound to compound; in *a*) resolution is 352, in most of the compounds resolution is about 100.

Each spectrum in Figure 5 is the result of averaging ion yield of 50 laser shots on a same sample spot. The differences in ion yield are due mainly to the non-uniformity of the contents of the

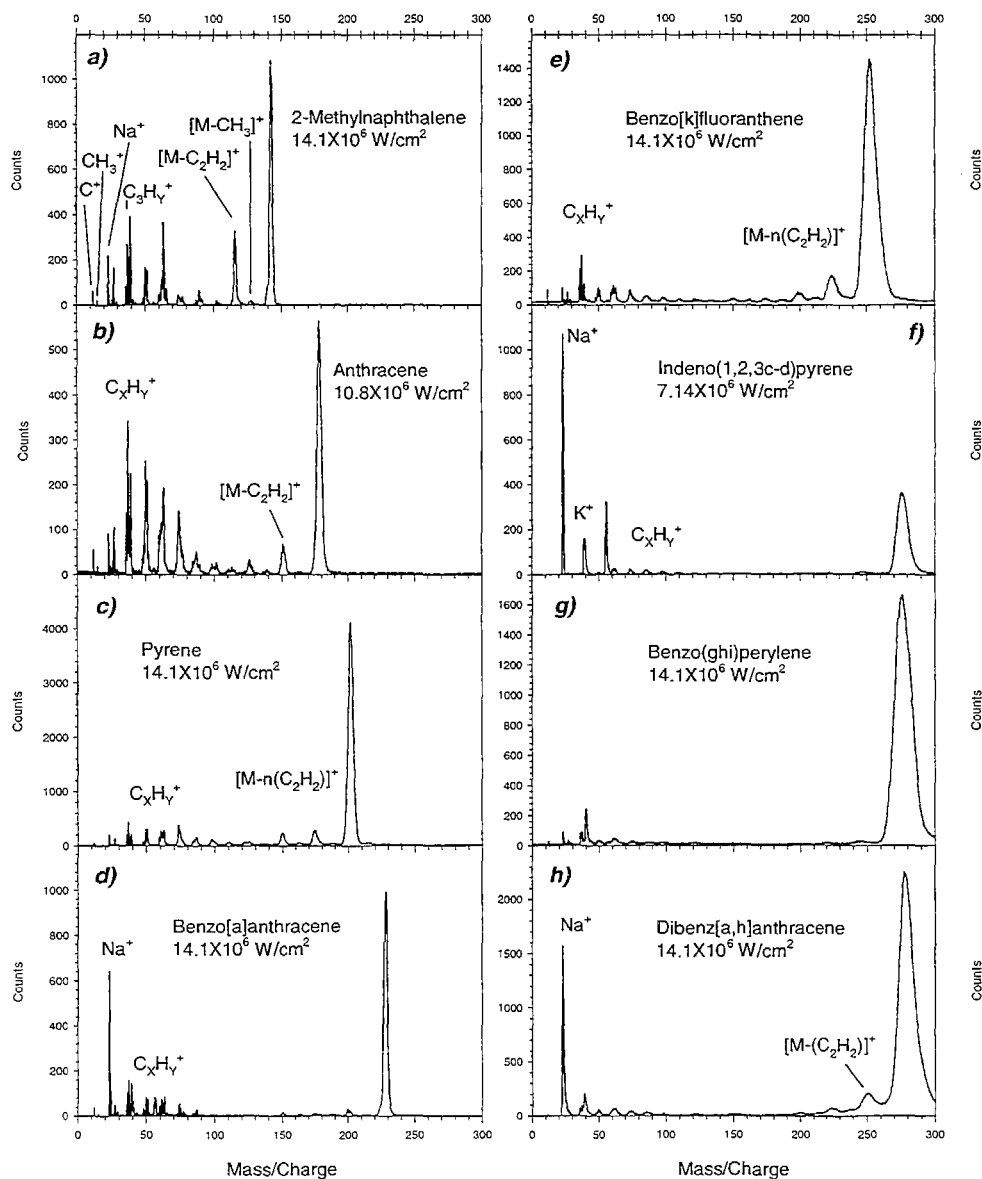


Figure 6. Excessive laser power yields significant fragmentation of PAHs. The molecular ion is the largest peak in the high mass range, however loss of C_2H_2 is also observed. Excessive laser power decreases resolution.

sample. As the solvent evaporates, the compound in solution crystallizes leaving an uneven distribution of crystals. The laser beam may illuminate spots with different crystal density in different samples. For all the compounds in Table II, we had positive results using power densities in the range of 1.3 to 2.4×10^6 W/cm^2 .

The pattern of fragmentation produced by PAHs at higher laser powers is, in most cases, distinctive of each compound. For most of the PAHs investigated, a fragmented molecular ion $[M - C_2H_2]^+$ appears (loss of an acetylene unit). Figure 6 shows the positive ion yield of 8 compounds (same set in Figure 5), using high laser power, 7.1×10^6 to 14.1×10^6 W/cm². The resolution at high mass range is reduced with increasing laser power.

At high laser powers (Figure 6) the low mass range is dominated by carbon fragments corresponding to C through C₇H₇. Fragmentation at high laser powers is problematic as it obscures the molecular ion peaks. A detail of the low mass ion yield for benzo[e]fluoranthene is shown in Figure 7. Ion C⁺, and chains C_xH_y⁺ are resolved up to mass 60. Na and K were used as markers for calibration purposes.

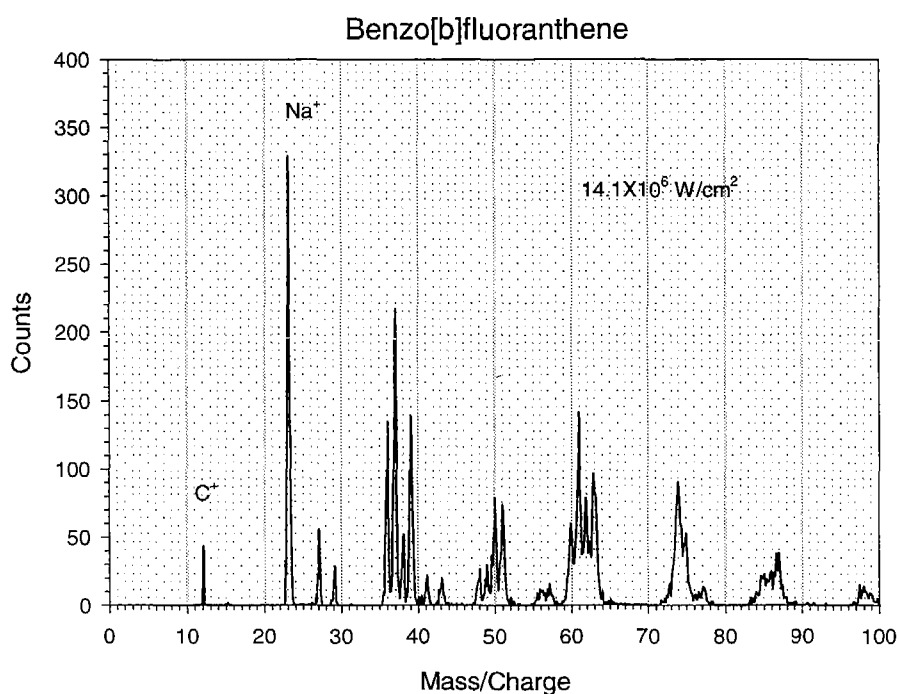


Figure 7. Low mass fragment yield of benzo[e]fluoranthene at 14.0×10^6 W/cm². Na and K were used as markers for calibration purposes. C, and C_xH_y chains dominate the ion yield for all PAHs investigated excessive laser power.

Naphthalene, acenaphthylene, and acenaphthene are difficult to analyze by LDI/TOFMS due to their high vapor pressure. The three low molecular weight compounds are rapidly pumped off the

sample probe in the vacuum of the instrument. Fortunately, naphthalene, acenaphthylene, and acenaphthene are easily detected by GC/MS.

LDI/TOFMS is very useful for high molecular weight PAHs that are difficult to analyze by conventional GC/MS methods.

IV.3 Spectra of Nitro-PAHs

Nitro PAHs in Table III (see Appendix C for molecular formula and structure) were examined by LDI/TOFMS. In general, nitro PAHs have electron affinities that are greater than 1 eV, so they may readily capture thermalized electrons to form stable negative ions. In contrast, PAHs do not form stable negative ions. The spectra collected for the target analytes of Table III are taken in negative mode for the detection of negative ions.

Table III

Nitro-PAHs targeted for MLD source test method development

| | |
|-------------------|---------------------|
| 1-nitropyrene | 4-nitropyrene |
| 2-nitropyrene | 2-nitrofluorene |
| 1,6-dinitropyrene | 5-nitroacenaphthene |
| 6-nitrochrysene | 2-nitrofluoranthene |
| 1,8-dinitropyrene | |

In our study, 266 nm laser shots of 8 ns time length were focused on samples of pure nitro-PAHs deposited on air filters. The power density used ranged from 1.3×10^6 to 14.1×10^6 W/cm² ($\pm 10\%$), corresponding to 0.5 to 7.2 μ J pulses of energy on 90-micron diameter spot. As in the case of PAHs spectra, resolution ($M/\Delta M$) varied from compound to compound, for most of the base peaks observed resolution was approximately 100 (Full width at half maximum value).

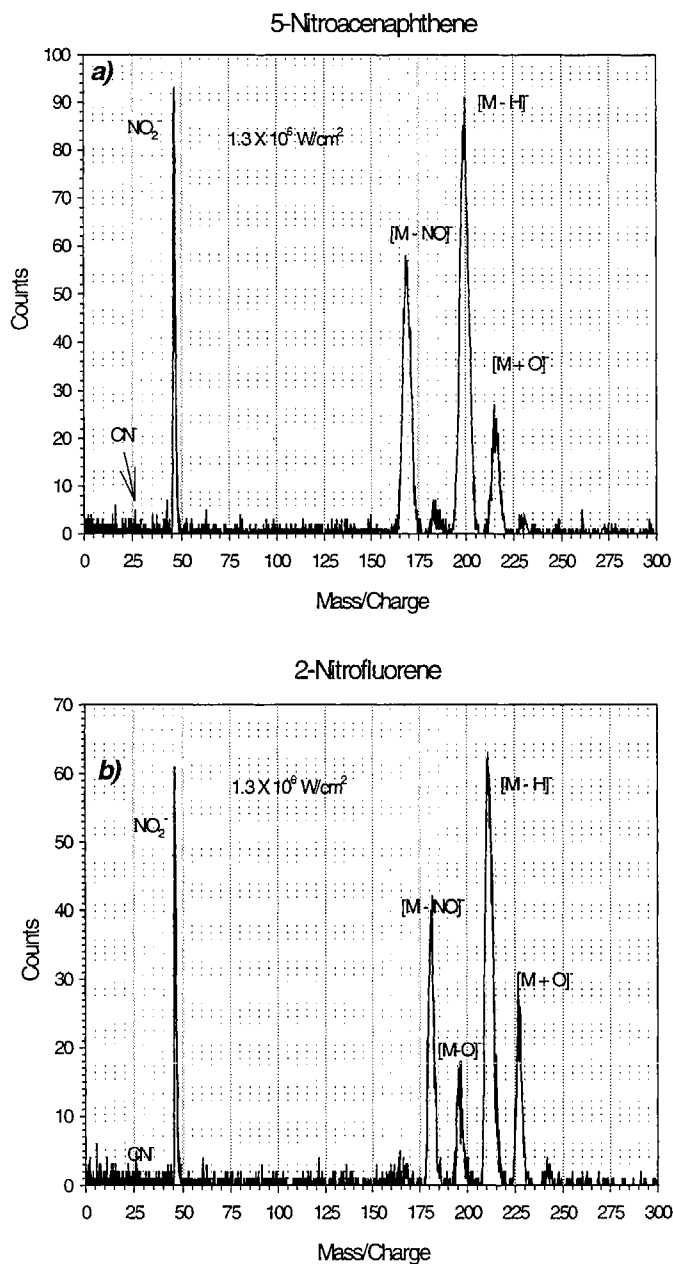


Figure 8. Negative ion yield of a) 5-nitroacenaphthene and b) 2-nitrofluorene. CN^- and NO_2^- appear in all spectra of nitro-PAHs. As result of the lost of an acidic proton at the carbon bridge between the benzene rings, the main peak observed is $[M-H]^-$.

laser shots on a single sample spot at a rate of 5 Hz. The most abundant high mass peak is $[M-H]^-$. Other peaks observed include a strong $[M-NO]^-$ and in less abundance, peaks that correspond to the gain and loss of 16 (one O) by the parent molecule.

Each of the nitro PAH compounds examined yielded a collection of high mass negative ion peaks, even at low laser powers. $[NO_2]^-$ and CN^- were detected in all cases; CN^- yield was much less intense than NO_2^- . Figure 8 shows negative ion spectra of 5-nitroacenaphthene and 2-nitrofluorene. The spectra correspond to the lowest power density employed, $1.3 \times 10^6 \text{ W/cm}^2$. Each spectrum was collected from the signal generated by 50

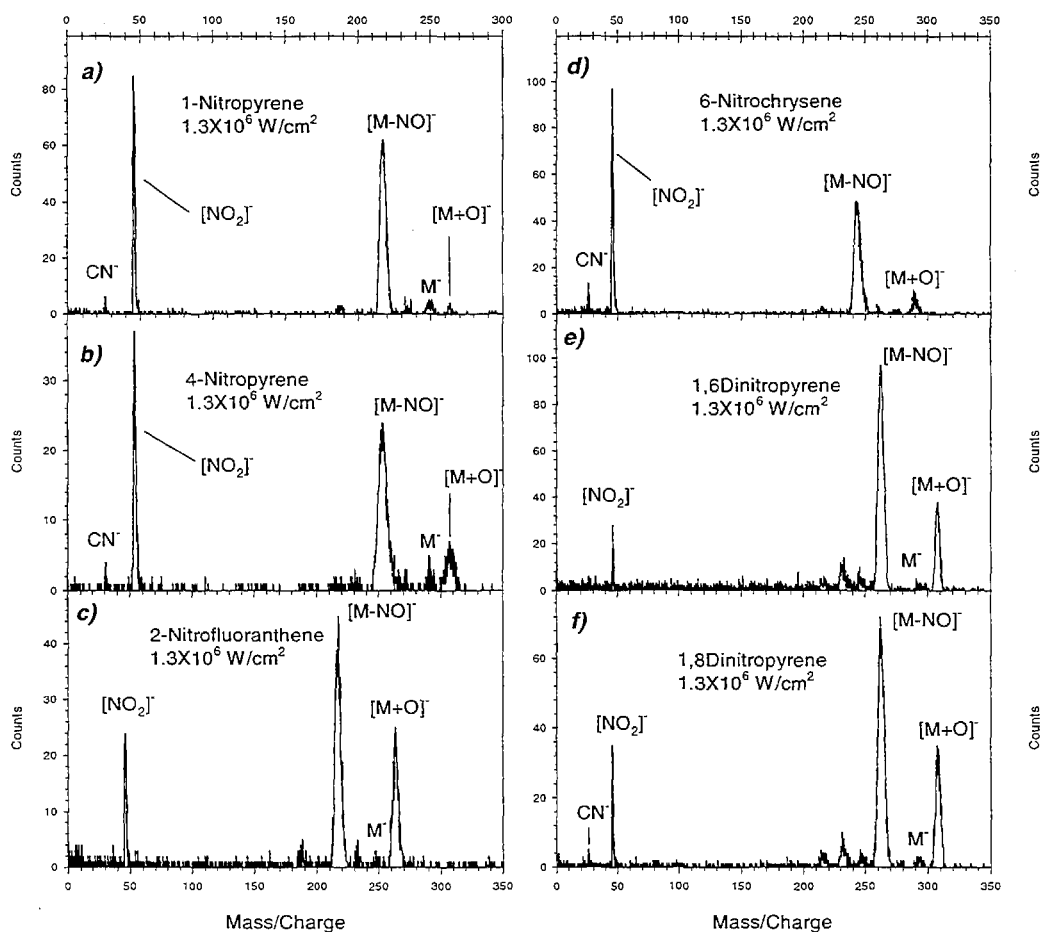


Figure 9. Negative ion yield of 6 different nitro-PAHs. Pure samples produce negative ion peaks corresponding to M^- and additional base peaks, mainly $[M-NO]^-$ and $[M+O]^-$. At low mass range, CN^- and NO_2^- appear as a signature of a nitro-PAHs

In contrast to the response of 5-nitroacenaphthene and 2-nitrofluorene, the other nitro-PAHs examined produce $[M - NO]^-$ as the main peak when the spectra are collected from the same spot at the sample. Figure 9 shows the negative ion spectra obtained from pure samples of 6 different nitro-PAHs: 1 and 4-nitropyrene, 2-nitrofluoranthene, 6-nitrochrysene, 1,6 and 1,8-dinitropyrene. The power density employed was $1.3 \times 10^6 \text{ W/cm}^2$ and each spectrum contains the

signal generated during 50 laser shots on the same sample spot. Other peaks produced include $[M + O]^-$ and in much less abundance $[M - O]^-$.

Qualitative differences in the spectra shown in Figures 8 and 9 suggest that the mechanisms of ionization of the parent ions are not the same. Nitro-acenaphthene and nitro-fluorene lose a relatively acidic proton from the carbon bridge between the two benzene rings, the resulting negative ion has the charge delocalized into the core of the molecule.

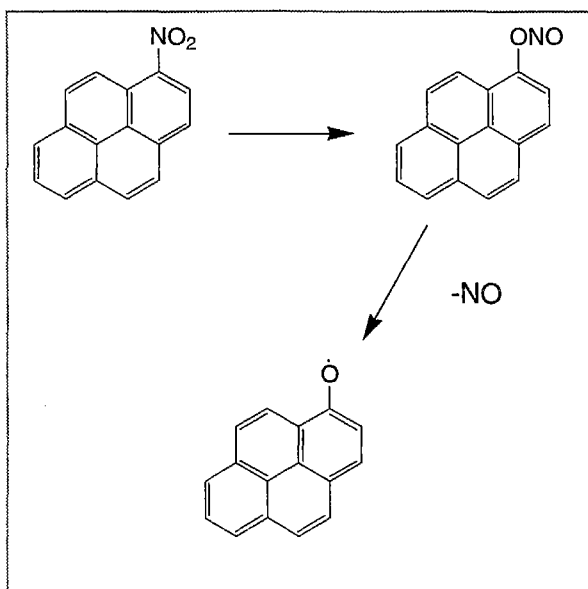
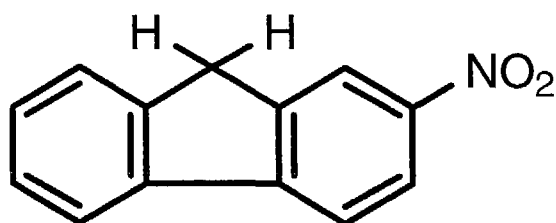
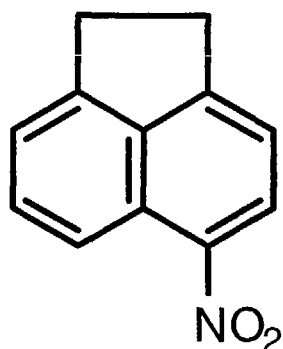


Figure 10. A possible pathway leading to the formation of $[M - NO]^-$ is illustrated here. Nitro-nitrite rearrangement involving the isomerization from $-NO_2$ to $-ONO$ following loss of NO

Nitro-fluorene



Nitro-acenaphthene



For the other nitro-PAHs examined in this work, all of them with structures composed by fused benzene rings, the mechanism of ionization occurs via electron capture producing a true molecular anion $[M]^-$. This is a secondary process that requires abundance of free electrons. The apparent destruction of the parent nitro-PAH is due to the need for significant laser power required to produce those free electrons, this condition causes greater photo fragmentation of

nitro-PAHs, leaving fewer intact molecules to compete for electrons in the plume.

The loss of NO from nitro-containing molecules has been postulated to proceed through a nitro-nitrite rearrangement mechanism [7]. The nitro-nitrite rearrangement involves

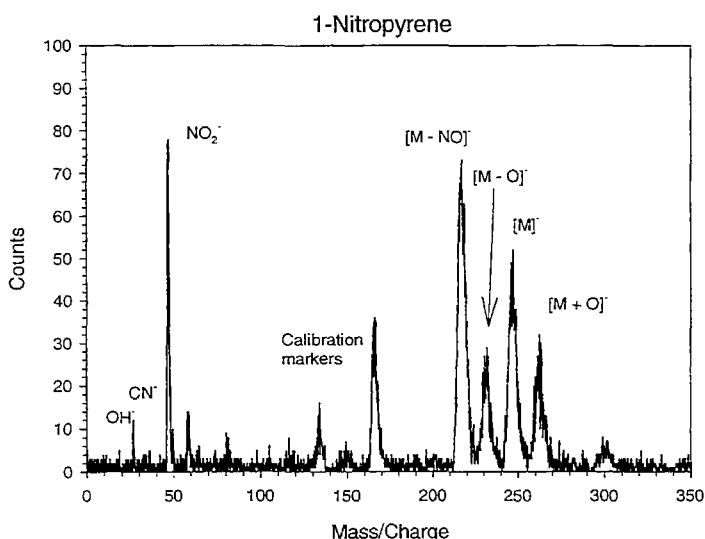


Figure 11. Negative ion yield spectrum of 1-nitropyrene. Sample probe was rotated during data acquisition. Molecular anion yield increase substantially respect to equivalent spectrum a) of Figure 11. Residual excitation may enhance mechanism that leads to the production of $[M - NO]^-$.

isomerization from $-NO_2$ to $-ONO$ at the carbon atom to which the nitro group was originally attached, see Figure 10. The subsequent loss of NO associated with electron capture yields the $[M - NO]^-$ ion.

The characteristic

peaks identified as NO_2^- and

CN^- were observed in all

negative spectra of the nitro-

PAHs examined. The neutrals

NO_2 and CN arise via photo dissociation of the nitro-PAHs, and these compounds having

electron affinities of 2.50 and 3.82 eV, respectively, will compete favorably in the capture of electrons.

Spectra shown in Figures 8 and 9 were taken from a single sample spot using a repetition rate of 5 Hz for the laser shots. In contrast in Figure 11 the sample was rotated as it was being irradiated resulting in illumination of *random spots* over the sample. An immediate intensification of the molecular anion is observed; however production of $[M - NO]^-$ is more

probable than production of $[M]$. Since nitro-nitrite rearrangement and loss of NO must occur within a single laser pulse, the intensity of the process may be a function of the pulse width.

Extremely short laser pulses may produce less $[M - NO]$.

IV. 4 Matrix effects

Matrix effects can play a significant role in relative ion yield, particularly for secondary processes. Environmental samples with high salt content can suppress formation of electron capture by organics. A salt content is less of a problem for direct photo ionization processes used for direct positive ion formation and detection.

Diesel soots. Diesel engine exhaust contains several PAHs and derivatives. The exact content of compounds varies with types of engine, fuels and operation conditions. For our test

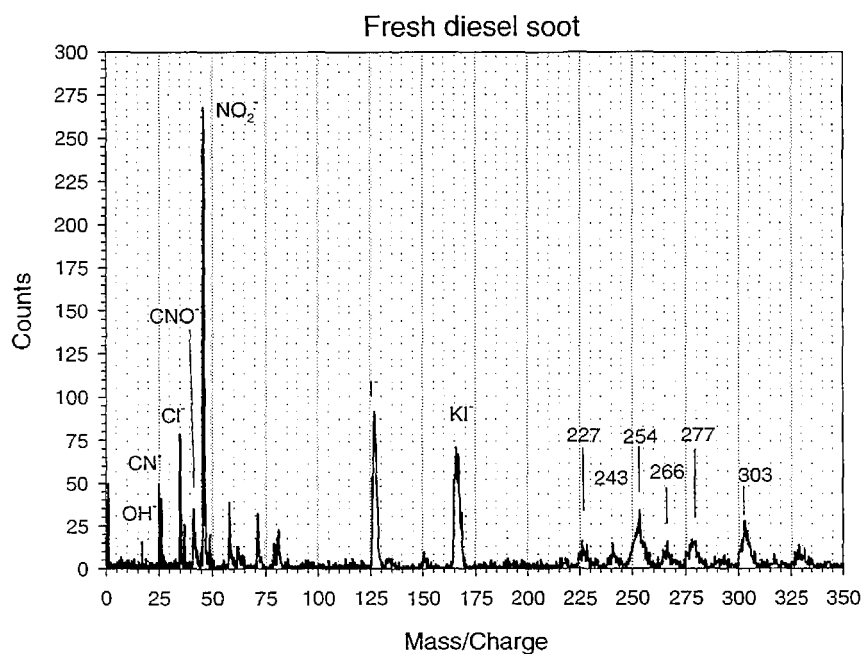


Figure 12. Negative ion yield from a sample of diesel soot obtained from cold start exhaust emissions. Several peaks appear in the mass range 200 to 350 dalton. Peaks have been tentatively identified as hydroxylated derivatives of PAHs (see text).

sample, we used a simple engine, air intake operating at atmospheric pressure and fueled with California reformulated diesel fuel (low in sulfur content). The sample was taken at the starting time and when the engine is cold. Under such circumstances, a diesel engine produces more soot than when the engine is warm and working at constant rate. Double side adhesive tape was used at the tip of the probe for holding a diesel sample of less than a mg. Figure 12 shows the negative ion spectrum obtained from the signal of 200 laser shots. The probe was rotated during exposure such that the laser shots were distributed randomly around a circle on the sample (see section III.1). At the low mass range, characteristic diesel peaks, OH⁻, CN⁻, NO₂⁻ are the most prominent expected peaks (I⁻ and KI⁻ were introduced as calibration markers). Chloride ions Cl⁻ (mass 35 and 37 at an isotopic ratio 3/1) appears as well. The lack of sulfate peak is not surprising as the fuel was low sulfur content (NIST diesel particulate matter 1650, produces a very intense HSO₄⁻ peak in negative mode).

Several peaks are observed in the range 200 to 350 mass units. We have identified tentatively the main peaks as PAHs derivatives: hydroxy-nitro-fluorene (mass 227), hydroxy-chrysene (mass 243), dihydroxy-nitro-anthracene (mass 254), hydroxy-perylene (mass 266), hydroxy-nitro-methyl-pyrene (mass 277) and hydroxy-nitro-methyl-chrysene (mass 303). Assignment of isomers would require LC analysis, however Figure 12 shows the potential of the technique for use as a tool of rapid screening for hydroxy and hydroxy-nitro derivatives of PAHs in environmental samples.

Environmental matrixes are extremely complex and in consequence in the process of electron capture, many different neutral species and fragments compete for free electrons. The results discussed above indicate that in negative mode, the detection of parent molecular anions of nitro-PAHs might be difficult due to interference of salts and other more electronegative

organic components. Failure to tune the mass spectrometer for best resolution also contributes to difficulty in detection of nitro-PAH that are expected to have lower intensity than hydroxy-nitro-PAH due to lower electron affinity. Improved resolution would yield improved sensitivity.

V. Conclusions

We have found an optimal range of laser power density that produces the maximum parent ion yield signal with a minimum of fragmentation for all PAHs and nitro-PAHs (Table II and Table III). A spectral library has been collected at that laser power density. Laser pulses of 266 nm and 8 ns duration with energies between 0.7 and 1.2 μJ (power density between 1.3×10^6 and $2.4 \times 10^6 \text{ W/cm}^2$) delivered to a sample spot of 90 μm diameter, produce molecular ion peaks that are easily identifiable without significant fragmentation.

All but three of the PAHs compounds of interest (see Table I), produce a main molecular ion peak without significant fragmentation. Naphthalene, acenaphthylene, and acenaphthene were not suitable for this kind of analysis due to their high vapor pressure, however these are readily detected by GC/MS.

Samples of pure compounds were prepared with a content of approximately 5 ng in an area covered by the laser beam. Our positive detection and identification of the sample compounds sets detection limits for LDI/TOFMS of at least 5 ng or better. Compounds with high electron affinity are more easily detected in negative ion spectra, while those with low ionization potential are more easily detected in positive ion spectra. Our detection limit is equal to or better than that of the High-Resolution Mass Spectrometry (HRMS) *practical quantitation limit* of ARB method 429. Thus our method can be used to screen samples for the presence of

PAH, but without the lengthy work up of Method 429. Cost savings can be realized by setting aside samples that do not have PAH detectable by LDI/TOFMS.

Negative ion spectra of nitro-PAHs produce several peaks associated to the parent molecule as well as NO_2^- and CN^- which are characteristic of all nitro-PAHs. The NO_2^- intensity is comparable to the peaks associated with the parent molecule. For two compounds, 5-nitroacenaphthene and 2-nitrofluorene, the main ion peak correspond to the molecule that has lost one proton. Other peaks include $[\text{M} - \text{NO}]^-$ and $[\text{M} + \text{O}]^-$. For the other nitro-PAHs investigated, the main peak observed was $[\text{M} - \text{NO}]^-$. Molecular anion yield was found to be very low when the same sample spot is continuously irradiated. Another important and distinctive peak associated with the parent ion with relative high yield was $[\text{M} + \text{O}]^-$.

Matrix effects were investigated spiking NIST Standard Reference Material Urban Dust with 1-nitropyrene. The results for nitro-PAHs are not as conclusive as for the PAH compounds. The main peak detected was $[\text{M} - \text{NO}]^-$ with an extremely low yield; the result of the experiment causes concern whether nitro-PAHs are or not detectable in environmental samples. An air sample might be quite different to one prepared using simple laboratory methods.

The laser power density range of 1.3 to $2.4 \times 10^6 \text{ W/cm}^2$ is optimal for detection of a wide range of PAHs and nitro-PAHs. The LDI/TOFMS method can be considered for implementation as a method for the direct screening of PAHs on particulate matter (PM10 and PM2.5) filters. A commercial LDI/TOFMS, with a sample probe modified to accommodate the particulate matter filter can be used to develop a standard Method for screening samples. The screening method would be used to determine which samples could be set aside as they would contain no detectable quantity of target compounds. The screening method would reduce both the cost and time required for large air quality studies by reducing the number of samples that require the

complete analysis. Negative ion detection is a secondary ion formation process, and is more sensitive to matrix effects

LDI/TOFMS in negative ion mode was used to investigate the contents of a sample of diesel soot. Peaks found are consistent with the detection of several hydroxylated varieties of PAHs. However the compound contents in the sample used are unknown and further studies are in progress for verification of the compounds detected.

Extraction and separation of the diesel components can be used to minimize matrix effects. Inorganic salts that interfere with organic negative ion formation can be removed. The polar organic components, which contain potentially biologically active compounds, could be screened in a manner similar to that used for pure nitro-PAHs compounds presented in the study.

VI. References

- [1] R. Bhatia, P. Lopipero and A.H. Smith, Diesel exhaust exposure and lung cancer, *Epidemiology* **9**, 84-91 (1998).
- [2] D. Schuetzle, T.E. Jensen, J.C. Ball, Polar PAH derivatives in extracts of particulates: biological characterization and techniques for chemical analysis. *Environ. Int.* **11**, 169-181 (1985).
- [3] Zimmermann R., Boesl U., Weickhardt C., Lenoir D., Schramm K.W., Kettrup A. and Schlag E.W., *Chemosphere*, **29**, 1877-1888 (1994).
- [4] W.C. Wiley and I.H. McLaren, Time-of-Flight Mass Spectrometer with Improved Resolution. *Rev. Sci. Instrum.* **26**, 1150-1157 (1955).
- [5] Young, M.K.G. Doctoral Dissertation, University of California, Davis, Decemeber 1991.
- [6] Smith, C.H. Doctoral Dissertation, University of California, Davis, December 1993.
- [7] R.N. Dotter, C.H. Smith, M.K. Young, P.B. Kelly, A.D. Jones, E.M. McCauley, and D.P.Y. Chang, Laser Desorption/Ionization Time-of-Flight Mass Spectrometry of Nitrated Polycyclic Aromatic Hydrocarbons. *Analytical Chemistry*, **68**, 2319-2324 (1996) and Dawit Z. Bezabeh, A. Daniel Jones, Lowell L. Ashbaugh, and Peter B. Kelly, Screening of Aerosol Filter Samples for PAHs and Nitro-PAHs by Laser Desorption Ionizaiton TOF Mass Spectrometry. *Aerosol Science and Technology* **30**, 288-299 (1999).

Appendix A. Time of flight

In a time of flight spectrometer, the mass difference is measured by the difference in the arrival time of the ions. All ions with the same electric charge receive the same kinetic energy. Assuming that an ion of mass m and charge q is formed with negligible initial velocity, the kinetic energy gained in absence of space charge effects is:

$$q|\Delta V_1| = \Delta E_{x1} = \frac{1}{2}mv_1^2 \quad \text{eq. A.1}$$

Where v_1 is its velocity at $x = x_1$ and $|\Delta V_1|$ is the electric potential drop between the plates. For detection of positive ions, V_0 is positive and $V_0 > V_1$; similarly for negative ions V_0 is more negative than V_1 . In the same way, the total kinetic energy that the ions gain between the source plate and the acceleration grid is,

$$q|V_0| = \Delta E_x = \frac{1}{2}mv_2^2 \quad \text{eq. A.2}$$

Where v_2 is its velocity at $x = x_2$ and $|V_0|$ is the potential drop between the source plate and acceleration grid. The acceleration of ions in the two regions of the source is:

$$a_1 = q \frac{|\Delta V_1|}{mx_1}, \quad \text{and} \quad a_2 = q \frac{|\Delta V_2|}{m(x_2 - x_1)} \quad \text{eq. A.3}$$

The total time that takes for an ion to reach the detector is the sum of the time for transit of each region of the spectrometer. The sum of the transit time of the three sections, source to extraction section, extraction acceleration section and the field free region is given by:

$$\Delta t = \Delta t_1 + \Delta t_2 + \Delta t_3 = \frac{v_1}{a_1} + \frac{v_2 - v_1}{a_2} + \frac{x_3 - x_2}{v_2} \quad \text{eq. A.4}$$

When substituting expressions for velocities and accelerations from equations A.1, A.2 and A.3, it is found that the total time for an ion to reach the detector at the end of the drift tube is:

$$\Delta t = F \left(\frac{m}{q} \right)^{\frac{1}{2}} \quad \text{eq. A.5}$$

where F is a parameter that depends on the grid spacing and applied voltage. For an instrument that is designed with rapid acceleration and a long drift region at the final velocity, the Δt_1 and Δt_2 can be neglected. Then F is given by:

$$F \cong \frac{(x_3 - x_2)}{(2V_0)^{1/2}}$$

In a time of flight mass spectrometer, typically Δt_1 and Δt_2 are very small when compared with Δt_3 . Ignoring the first two terms in equation A.4, the expression for the time of flight is:

$$\Delta t \cong \frac{(x_3 - x_2)}{(2V_0)^{1/2}} \left(\frac{m}{q} \right)^{1/2} \quad \text{eq. A.6}$$

Which yields the result that the ratio m/q is proportional to Δt^2 .

Appendix B. Mass calibration of ion spectra

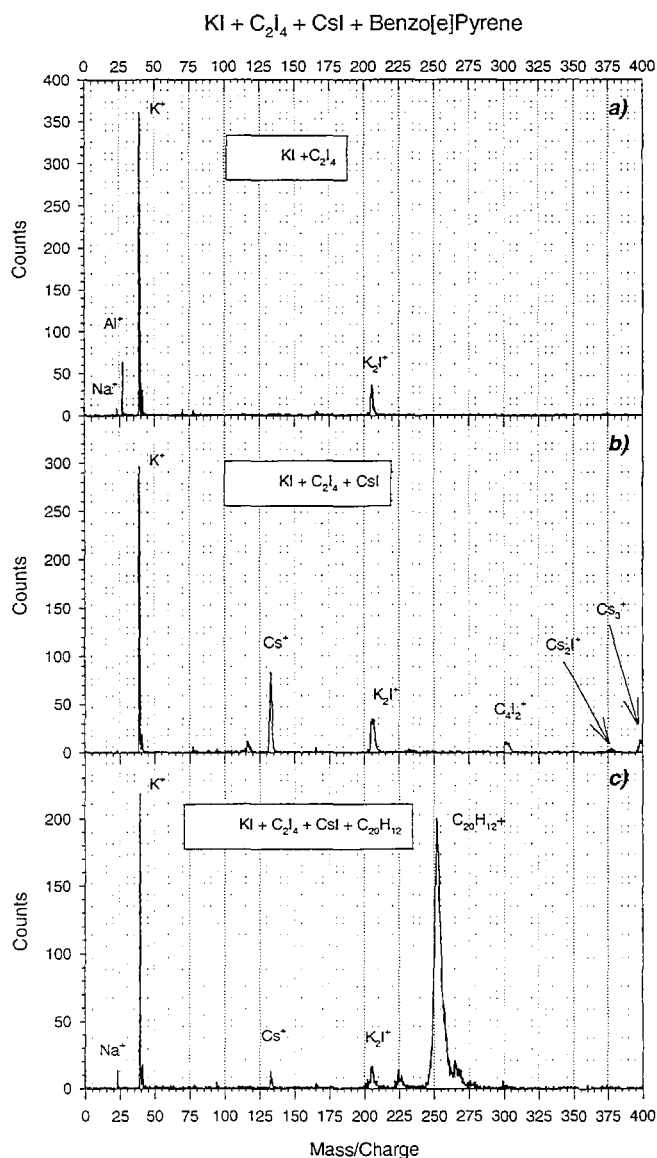


Figure B.1. Positive intensity ion peaks belonging to known compounds are identified. Pairs of time squared-mass for each identified peak are used for finding a calibration function. In this plot, different mixtures were used together with Benzo[e]pyrene in 3c. Mass and charge are given in units of mass and charge

Raw LDI/TOFMS spectra consist of signal intensity versus flight of time (see section II.2). Since mass is proportional to the square of flight time in a TOF mass spectrum, the data files are stored as flight time squared and intensity data-pairs. A primary mass calibration was determined by examination of standard compounds. The primary calibrations were used as a guide for performing the final calibration for each sample of PAHs and nitro-PAHs compounds examined.

Figure B.1 shows positive ion yield calibrated mass spectra obtained from pure compounds used as calibration standards. As LDI/TOFMS is sensitive only to mass, a careful initial mass calibration requires the use of several compounds, which yields masses covering the range of mass of interest. Compounds containing K and Cs produce several positive ion peaks in the mass range up to 400 units of mass. Benzo[e]pyrene (mass

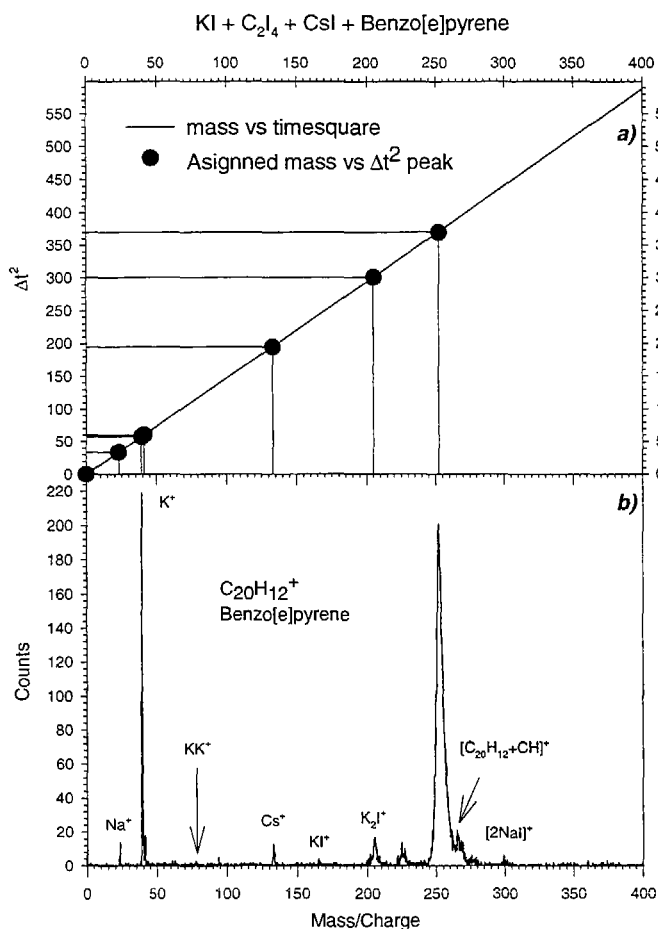


Figure B.2. Pairs of mass of identified peaks-time square follow an almost linear relation. In a) and b) the red line is used for the linear fitting, in black line appears the second order polynomial fitting. The difference is hardly noticeable for low yield, as in this case.

In Figure B.2, eq. B.1 was used for calibration. The difference between a linear and a second order polynomial fitting is almost not noticeable for this case in which the total ion yield is very low. In general the precision of the calibration was within 1-2 daltons.

252.34 dalton) is easily identified in 3c) using the primary calibration obtained with the reference compounds.

According to eq. A.6, mass (m) is linearly proportional to the square of the arrival time (Δt^2). However due to space charge effects at the plume of desorbed material (containing neutrals, ions and electrons), the effective mean field differs from the field set up by the bias applied to the repeller and extractor plates. In order to correct for those effects, it is necessary a second order polynomial between mass and time square:

$$m = a(\Delta t^2)^2 + b(\Delta t^2) + c$$

eq. B.1

In Figure B.2, eq. B.1 was used for

Appendix C. Selected information

Table C.1
Molecular formulas and structures of PAHs

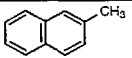
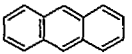
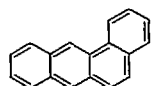
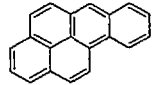
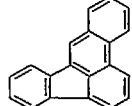
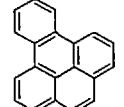
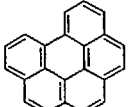
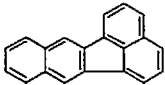
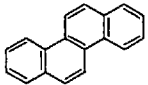
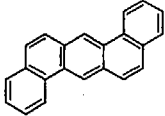
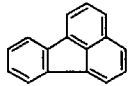
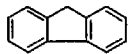
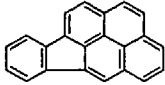
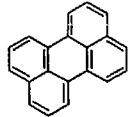
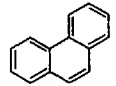
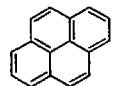
| Compound | Molecular Formula | Molecular Weight | Ionization Potential (eV) [†] | Structure |
|----------------------|---------------------------------|------------------|--|---|
| 2-Methylnaphthalene | C ₁₁ H ₁₀ | 142.20 | |  |
| Acenaphthylene | C ₁₂ H ₈ | 152.19 | 8.778 |  |
| Acenaphthene | C ₁₂ H ₁₀ | 154.21 | 8.525 |  |
| Anthracene | C ₁₄ H ₁₀ | 178.23 | 8.049 |  |
| Benzo[a]anthracene | C ₁₈ H ₁₂ | 228.29 | 8.111 |  |
| Benzo[a]pyrene | C ₂₀ H ₁₂ | 252.32 | 7.83 |  |
| Benzo[b]fluoranthene | C ₂₀ H ₁₂ | 252.32 | |  |
| Benzo[e]pyrene | C ₂₀ H ₁₂ | 252.32 | 8.137 |  |
| Benzo[ghi]perylene | C ₂₂ H ₁₂ | 276.34 | 7.943 |  |

Table C.1 (Continuation)

| | | | | |
|------------------------|----------------|--------|-------|---|
| Benzo[k]fluoranthene | $C_{20}H_{12}$ | 252.32 | 8.167 |  |
| Chrysene | $C_{18}H_{12}$ | 228.29 | 8.261 |  |
| Dibenz[a,h]anthracene | $C_{22}H_{14}$ | 278.35 | 8.148 |  |
| Fluoranthene | $C_{16}H_{10}$ | 202.26 | 8.466 |  |
| Fluorene | $C_{13}H_{10}$ | 166.22 | 8.609 |  |
| Indeno[1,2,3-cd]pyrene | $C_{22}H_{12}$ | 276.34 | 8.024 |  |
| Naphthalene | $C_{10}H_8$ | 128.2 | 8.575 |  |
| Perylene | $C_{20}H_{12}$ | 252.32 | 7.846 |  |
| Phenanthrene | $C_{14}H_{10}$ | 178.23 | 8.479 |  |
| Pyrene | $C_{16}H_{10}$ | 202.26 | 8.029 |  |

*R.A. Hites and W.J. Simonsick: *Calculated Molecular Properties of Polycyclic aromatic hydrocarbons*, Elsevier, Amsterdam, 1987.

Table C.2
Molecular formulas and structures of Nitro PAHs

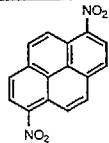
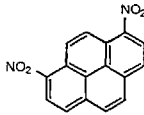
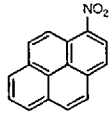
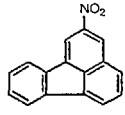
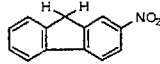
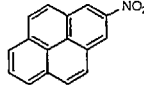
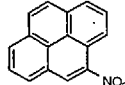
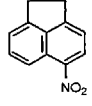
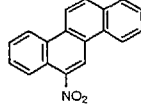
| Compound | Molecular Formula | Molecular Weight | Structure |
|---------------------|--------------------|------------------|---|
| 1,6-Dinitropyrene | $C_{16}H_8N_2O_4$ | 292.25 |  |
| 1,8-Dinitropyrene | $C_{16}H_8N_2O_4$ | 292.25 |  |
| 1-Nitropyrene | $C_{16}H_9NO_2$ | 247.25 |  |
| 2-Nitrofluoranthene | $C_{16}H_9NO_2$ | 247.25 |  |
| 2-Nitrofluorene | $C_{13}H_9NO_2$ | 211.22 |  |
| 2-Nitropyrene | $C_{16}H_9NO_2$ | 247.25 |  |
| 4-Nitropyrene | $C_{16}H_9NO_2$ | 247.25 |  |
| 5-Nitroacenaphthene | $C_{12}H_9NO_2$ | 199.21 |  |
| 6-Nitrochrysene | $C_{18}H_{11}NO_2$ | 273.29 |  |

Table C.3

Electron affinity of selected atoms and molecules*

| Atom, Molecule | Electron Affinity (eV) |
|--------------------------------|------------------------|
| Cl | 3.613 |
| I | 3.078 |
| C | 1.25 |
| S | 2.077 |
| CN | 3.82 |
| CS | 1.2 |
| Cl ₂ | 2.5 |
| ClO | 1.95 |
| I ₂ | 2.6 |
| NaCl | 0.67 |
| NO | 0.024 |
| OH | 1.83 |
| SO | 1.09 |
| C₂H | 3.73, 2.7 |
| C ₃ | 2.5 |
| CNS | 1.99 |
| NO₂ | 2.50 |
| O ₃ | 2.1 |
| SO ₂ | 1.0 |
| CH ₃ | 1.08 |
| CO ₃ | 2.69 |
| NO₃ | 3.7 |
| SO₃ | 1.70 |
| CO ₄ | 1.22 |
| HNO ₃ | 0.57 |
| C ₂ Cl ₅ | 1.55 |
| Benzene | -1.15 |
| Naphthalene | -0.06 |
| Anthracene | 0.49 |
| Nitrobenzene | 1.01 |
| 1-Nitronaphthalene | 1.23 |
| 9-Nitroanthracene | 1.43 |

*B.M. Smirnov, Negative Ions. McGraw-Hill International Book Company, New York 1982.

Appendix D. CHARACTERIZATION OF CHEMICAL COMPOSITION AND SIZE OF DIESEL EXHAUST PARTICULATE MATTER BY LDITOF/MS.

J. Suro*, Q. Chen, I.M. Kennedy, T.A. Cahill and P.B. Kelly
University of California, Davis, California 95616

Introduction

Diesel engines see extensive use due to their high efficiency and suitable torque characteristics. In general diesel engines have lower carbon monoxide and hydrocarbon emissions than spark-ignition engines. However, they are known to create much larger amounts of particulate matter and polycyclic aromatic hydrocarbons (PAHs) and their derivatives. Contributing factors are higher temperatures and pressures in the combustion process together with larger initial concentrations of aromatics in the diesel fuel.

The presence of the aromatic compounds in the particulate matter represents a potential hazard to human health. Several PAHs and nitro-PAHs have been identified as carcinogenic compounds [D1]. The extent of human exposure to PAHs and their derivatives depends on the partitioning between the gas and particle phases as well as the size distribution of the particle fraction containing the PAHs. There is a greater potential health impact if the PAHs are components of particles that penetrate and deposit into the bronchia and alveoli of the lungs. Studies show that a major fraction of particles that are 1.0 μm or less in diameter penetrate into the air ways and lungs [D2]. Moreover, recent studies have correlated health effects with the concentration of atmospheric particles, yet have failed to identify the causative agents [D3]. Since the toxicity of particles from different sources varies widely, such studies would be much more valuable if the particles from a source were characterized with respect to size and composition.

Traditional methods for the determination of PAHs and nitrated PAHs are based on gas chromatography/mass spectrometry or liquid chromatography with fluorescence techniques for detection. Both approaches are time consuming, may require solvent extraction and separation, are expensive, and in most cases require multiple runs [D4]. In this study, we demonstrate the applicability of Laser Desorption Ionization Time of Flight Mass Spectrometry (LDITOF/MS) as a rapid screening method in the analysis of diesel exhaust particulate matter collected and segregated by particle size using a multiple stage portable impactor. LDITOF/MS is used to generate parent ion dominated spectra with low fragmentation from samples containing particles in a specific size range, which makes LDITOF/MS an excellent technique for the screening for PAHs in complex mixtures without need for solvent extraction and separation.

Experimental

The source of diesel exhaust particulate matter was a direct injection Wisconsin Robin 1 cylinder diesel engine, model WRD1-270, aspirated at normal pressure (no turbocharger was used). Samples were collected with the engine idling warm at 2,000 rpm. Reformulated California grade diesel fuel (low sulfur content) was used for the experiment.

Diesel soot samples were collected using a three stage portable impactor developed by the Delta Group at UC Davis [D5]. The impactor was equipped with aluminum foil strips attached to rotary drums that, during sampling, rotated at a fixed angular speed exposing the attached aluminum strip to an inlet nozzle. The dimensions of the inlet nozzle determined the range of size of particles collected on the surface of the strip. As the drum rotates the segment of aluminum strip exposed to the inlet changed continuously, resulting in a deposition of sample with a time reference. Samples were obtained positioning the impactor at 20 cm from the exhaust of the diesel engine. A Nucleopore® filter at the external inlet prevented coarse matter from entering the impactor, trapping particles $> 2.5 \mu\text{m}$ of diameter. Particles with aerodynamic diameter between $2.5 \mu\text{m}$ to $1.15 \mu\text{m}$ were collected on the first stage of the impactor (denoted stage A). The second stage collected particles within the size range $1.15 \mu\text{m}$ to $0.24 \mu\text{m}$ (denoted stage B). The third stage accumulated particles of size $0.24 \mu\text{m}$ to $0.07 \mu\text{m}$ (denoted stage C). The 50% cut point of such an impactor has been validated both in extensive field and laboratory studies [D5] and references there in). Particles not trapped on the aluminum strips were collected on a $0.01 \mu\text{m}$ porous teflon filter at the impactor outlet.

The laser desorption ionization time of flight mass spectrometer has been described in previous publications [D6]. The fourth harmonic of a Nd:YAG laser, 266 nm, with a 2.5 ns pulse width was used to desorb and ionize the sample. The UV laser beam was focused into the source region through a 250 mm focal length S1-UV quartz lens. The beam was directed incident to the sample surface at 45° . Neutral density optical filters were used to reduce the laser power to 10^6 W/cm^2 at the focal point on the sample surface. The beam diameter at the focal point was about $90 \mu\text{m}$. A time delay of 250 ns in the application of the extraction potential at the source allowed time for prompt decay of metastable ions and improved overall resolution.

Particulate matter from each stage and as well as the inlet and outflow filters of the impactor were analyzed using LDITOF/MS. Segments of the aluminum foil from the impactor were attached to the sample probe and loaded into the LDITOF/MS. Each spectrum recorded was the sum of 240 randomly located laser shots. Blank filters and aluminum foil were checked for contaminants. Both positive and negative ion mass spectra were collected and analyzed.

Results

Positive ion mass spectra for five diesel particle size ranges matter are shown in Figure 1. Spectrum in *1a*) was obtained from the particles trapped at the external inlet filter with diameters larger than $2.5 \mu\text{m}$; *1b*) shows the spectrum resulting from particles with aerodynamic diameter between $2.5 \mu\text{m}$ to $1.15 \mu\text{m}$, stage A; *1c*) from the size range $1.15 \mu\text{m}$ to $0.24 \mu\text{m}$, stage B; *1d*) was obtained from particles in the stage C whose diameters range between $0.24 \mu\text{m}$ and $0.07 \mu\text{m}$. At the bottom *1e*) display the ion yield obtained from the outlet filter, with particles smaller than $0.07 \mu\text{m}$.

Low mass PAHs are more abundant in large particles, $> 2.5 \mu\text{m}$ diameter, than small particles, $< 0.07 \mu\text{m}$ diameter. The general trend of the shift of PAH mass, with high mass PAH being associated with the fine particulate is observed in Figures *1a*) through *1e*). Only the smallest particles, $0.07 \mu\text{m}$ have significant amounts of PAH with mass greater than 400 Da.

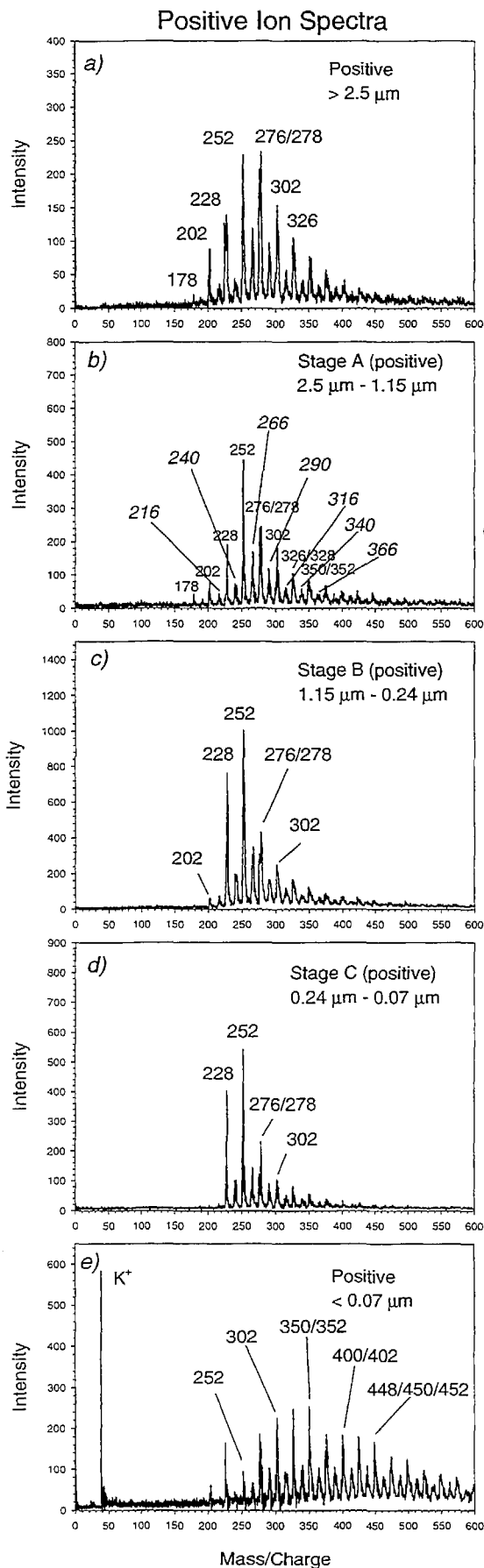


Figure 1. Positive ion mass spectra for five diesel particle size ranges.

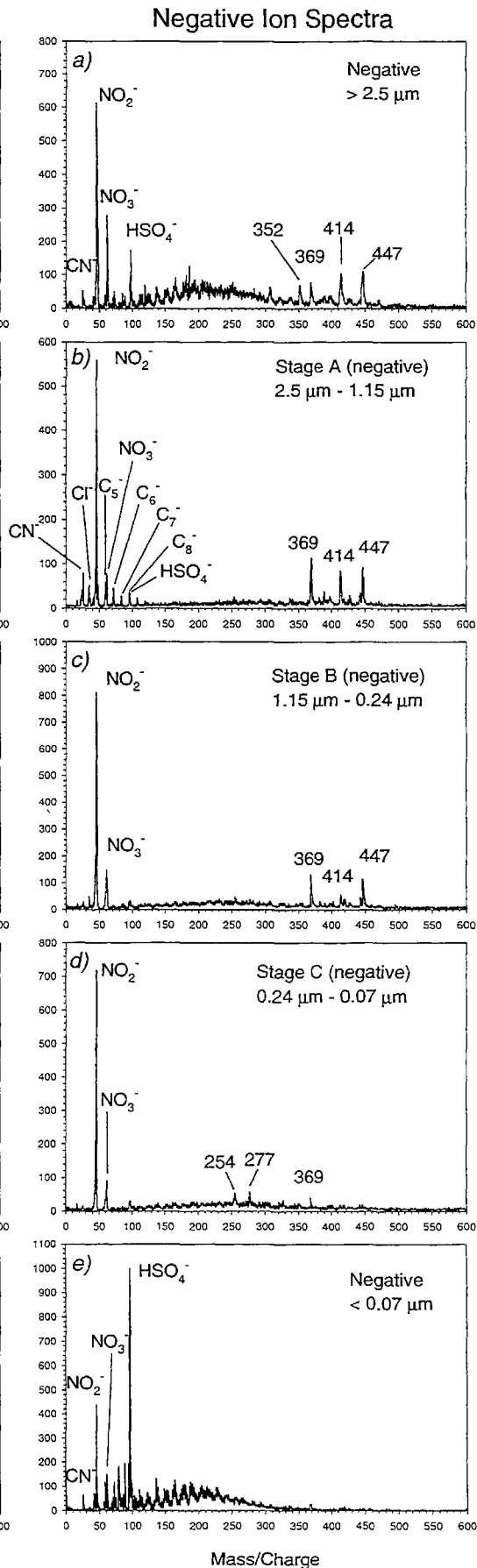


Figure 2. Negative ion mass spectra for five diesel particle size ranges.

Table I Common PAHs in diesel soot.

| PAH | Mass (Da) |
|----------------------|-----------|
| phenanthrene | 178 |
| fluoranthene | 202 |
| pyrene | 202 |
| benz[a]anthracene | 228 |
| chrysene | 228 |
| benzo[a]pyrene | 252 |
| benzo[e]pyrene | 252 |
| benzo[k]fluoranthene | 252 |
| perylene | 252 |
| benzo[ghi]perylene | 276 |
| indeno[123-cd]pyrene | 276 |

Two series of PAH ions are observed in all the positive ion spectra in Figure 1. The two series are most apparent in Figure 1e). The first series is comprised of m/z : 178, 202, 228, 252, 276/278, 302, 326/328, 350/352, 374/376, 398/400/402, and higher masses. The second series has twice the frequency as the first series, with every other peak overlapping with the first series. The second series is comprised of m/z 190, 202, 216, 226, 240, 252, 266, 276, 290, 302, 316, 326, 340, 350/352, 366, and higher masses. Both series have been labeled in Figure 1b). A surprisingly large potassium signal is observed in the smallest particles, Figure 1e).

Negative ion spectra of the diesel particulate matter are shown in Figure 2. As in the case of the spectra of positive ions, each plot corresponds to a different fraction. In contrast to positive ion spectra, the highest mass negative ions (m/z : 369, 414, and 447) are associated with the larger particles. Inorganic ions, OH^- , Cl^- , NO_2^- and NO_3^- are observed for all five particle size range. Ultrafine particulate, $< 0.07 \mu\text{m}$, show significantly higher HSO_4^- than larger particles.

Discussion

In a recent study by Reilly and collaborators [D7], organic composition of individual particles of diesel soot are obtained using an excimer laser for ablation and ionization. Using this technique they are able to detect known compounds in diesel soot and to establish some differences in chemical composition according to particle size. However that method involves unavoidable fragmentation that obscures their results. Another study, Hankin and John [D8] examined the chemical composition of individual particles of diesel soot SRM 1650. In their experiment using TOF/MS, individual particles fixed to a sample support are subject to microlaser beam that desorbs compounds from the particle, and a second beam ionizes the compounds in the plume of desorbed material. The Hankin and John TOF/MS analysis of SRM 1650 yielded the mass of some certified compounds in this sample as well as some other compounds not certified but known to be present in such standard such as alkylated PAHs. The Hankin and John study examined only very large particles ($\sim 20 \mu\text{m}$).

In our study we report the first mass spectra of particles that were sized using an impactor. The mass spectra are the summation of 240 laser shots at different points on the sample surface. Each laser spot was $90 \mu\text{m}$ diameter, which would ablate material from many $1 \mu\text{m}$ diameter particles. The signal was derived from many particles, thus obtaining reproducible results that are representative of a particular particle size range. In positive ion mode, the most intensive low mass peaks in Figure 1 correspond to PAHs commonly found in diesel exhaust listed in Table I. Moreover from Figure 1, it is clear that many other PAHs are present in the samples. The first

series corresponds to graphite-like PAHs isomers containing only 6 member rings. The second series, with every other peak overlapping with the first series, corresponds to PAHs containing five member rings. Spectra in Figure 1 shows identifiable peaks up to mass 448. Table II list a few possible assignments to peaks in the second series [D9].

The spectra obtained from the 1.15 – 2.5 μm impactor sample is extremely similar to that of Filter II of our previous work [D6b] sampling PM 2.5 at the Sacramento bus station. In Filter II, methyl PAH were observed in positive ion spectra, while nitro PAH were absent in the negative ion spectra. The lack of detection of nitro-PAH in Filter II, in contrast to detection in Filter I and Filter III was interpreted as due to variation in the exhaust of the different buses in the terminal at the time the samples were taken. Similarly, the lack of detection of nitro-PAH in the impactor study indicates that the engine was tuned such that it did not emit significant amounts of nitro-pyrene or other nitro-PAH identified in the PM 2.5 study.

Soot particles emitted from a diesel engine are usually observed as chain aggregates composed of several tens to hundreds of primary spherical particles. Using electron microscopy, Ishiguro et

Table II. Other PAH in the second series

| Formula | Mass (Da) | Compounds |
|------------------------------|-----------|---|
| $\text{C}_{16}\text{H}_{10}$ | 202 | Fluoranthene |
| $\text{C}_{17}\text{H}_{12}$ | 216 | Cyclopentaphenanthrene Cyclopentaanthracene Benzofluorene |
| $\text{C}_{18}\text{H}_{10}$ | 226 | Benzo(ghi)fluoranthene |
| $\text{C}_{19}\text{H}_{12}$ | 240 | Cyclopentapyrene Benzofluoranthene Cyclopentachrysene Benzopyrene |
| $\text{C}_{20}\text{H}_{12}$ | 252 | Benzocyclopentantracene |
| $\text{C}_{21}\text{H}_{14}$ | 266 | Benzocyclopentantracene Indenophenanthrene Dibenzofluorene Benzochrysene |
| $\text{C}_{22}\text{H}_{12}$ | 276 | Benzocyclopentapyrene |
| $\text{C}_{23}\text{H}_{14}$ | 290 | Benzocyclopentachrysene Dibenzopyrene |
| $\text{C}_{24}\text{H}_{14}$ | 302 | Cyclopentindenophenanthrene |
| $\text{C}_{25}\text{H}_{16}$ | 316 | Benzindenophenanthrene |
| $\text{C}_{26}\text{H}_{14}$ | 326 | Indenoperylene |
| $\text{C}_{27}\text{H}_{16}$ | 340 | Tribenzopyrene |
| $\text{C}_{28}\text{H}_{14}$ | 350 | Diindenopyrene |
| $\text{C}_{29}\text{H}_{18}$ | 366 | Dibenzopentacene |

al.[D10] found that the structure of such spherical particles consist of an inner core surrounded by an outer shell. The inner cores of 0.010 μm of average diameter are composed of nonplanar molecules. The surrounding outer shell is composed of micro crystallites comprising several polycyclic aromatic hydrocarbon layers oriented concentrically in a soot particle. During shell formation, molecules, radicals, or ions including two to four carbon atoms could contribute the surface reactions promoting the polycyclic growth of the graphitic crystallites. The LDITOF/MS results may yield insight to soot formation by examination of the smallest particles. The observation of K^+ and HSO_4^- suggests that the small particles may have nucleated around a potassium bisulfate core. The extreme high mass range of PAHs observed for small particles would not be observable by traditional GC/MS.

Diesel soot particles exhibit sizes ranging) from 4 μm to 0.04 μm , with a peaking distribution about 0.1 μm [D11]. Our study reveal that there are differences in the chemical composition of the particles within this range. Chemical speciation of particles is important for toxicological studies that assess the health hazard imposed by the continuous use of diesel engines. Toxicological assessments, regulation and development of cleaner running diesel engines [D12] require development of analytical methods that can examine the exhaust by particle size.

Conclusions

The ability of LDITOF/MS to characterize the chemical composition of diesel soot particles that were sized using an impactor has been demonstrated. Results indicate a variation of the chemical composition with particle size. In general finer particles have a high concentration of extremely large PAHs, potassium, and sulfate. The larger particles contain lower mass PAHs. Our data show the presence of many PAHs in diesel exhaust that have not been fully characterized as compounds found in diesel soot, including extremely large PAHs not amenable to GC/MS analysis.

Our technique can be used to characterize different sources according to the size of the particles. Accurate assessment of human health hazards associated with particulate matter requires chemical analysis associated with particle size and source. Such information would be very valuable for addressing the question of bioactivity associate with different classes of particles.

References

- D1. R. Bhatia, P. Lopipero and A.H. Smith, Diesel exhaust exposure and lung cancer, *Epidemiology* 1998, **9**, 84.
- D2. US Environmental Protection Agency, 1996. Air quality Criteria for Particulate Matter, vol. I, EPA/600/P-95/001aP, Washington, DC.
- D3. Dockery, D.W.; Schwartz, J.; Spengler, J.D. Air pollution and daily mortality – associations with particulates and acid aerosols. *Environ. Res.* 1992, **59**, 362.
- D4. Scheepers, P.T.J., Velders, D.D., Martens, M.H.J., Noordhoek, J., Bos, R.P. Gas chromatographic-mass spectrometric determination of nitro polycyclic aromatic hydrocarbons in airborne particulate matter from workplace contaminated with diesel exhaust. *J. Chromatogr. A* 1994, **A 677**, 107.
- D5. Malm, W.C., Sisler, J.F., Huffman, D., Eldred, R.A. and Cahill, T.A. Spatial and seasonal trends in particle concentration and optical extinction in the United States. *J. Geophys. Res.*, 1994, **99**, Sec. D, 1347.
- D6a. Bezabeh, D.Z., Allen, T.M., McCauley, E.M. and Kelly, P.B. Laser desorption ionization time of flight mass spectrometry of nitrated polycyclic aromatic hydrocarbons. *J. Am. Soc. Mass Spect.*, 1997, **8**, 630.

- D6b. Bezabeh, D. Z., Jones, A. D., Ashbaugh, L. L., and Kelly, P.B. Screening of Aerosol Filter Samples for PAHs and Nitro-PAHs by Laser Desorption Ionization TOF Mass Spectrometry. *Aerosol Science and Technology* 30, 288-299 (1999).
- D7. Reilly, P.T.A., Gieray, R.A., Whitten, W.B., and Ramsey, J.M. Real time characterization of the organic composition and size of individual diesel engine smoke particles. *Environ. Sci Technol.* 1998, **32**, 2672.
- D8. Hankin, S.M. and John P. Laser time of flight mass analysis of PAHs on single diesel particles. *Anal. Chem.* 1999, **71**, 1100.
- D9. Sander, L.C. and Wise, S.A. Polycyclic Aromatic Hydrocarbon Structure Index. NIST Special publication 922. 1997.
- D10. Ishiguro, T.; Takatori, Y. and Akihama K. Microstructure of diesel soot particles probed by electron microscopy: first observation of inner core and outer shell. *Combustion and Flame*, 1997, **108**, 231.
- D11. Kerminen, V.M. et. al. Characterization of the particle phase in the exhaust from diesel car. *Environ. Sci. Technol.* 1997, **31**, 1883.
- D12. Rakopoulos, C.D.; Hountalas, D.T.; Taklis, G.N. and Tzanos, E.I. Analysis of combustion and pollutants formation in a direct injection diesel engine using a multi-zone model. *International Journal of Energy Research*, 1995, **19**, 63.